Selectively doped germanium THz laser

M. V. Dolguikh, A.V. Muravjov, R. E. Peale
Dept. of Physics, University of Central Florida, Orlando FL, 32816-2385

ABSTRACT

Monte Carlo simulation of carrier dynamics and far-infrared absorption was performed to test the importance of electron-electron interaction in selectively doped multi-layer p-Ge laser at high doping concentration. The laser design exploits the known widely tunable mechanism of THz amplification on inter-sub-band transitions in p-Ge, but with spatial separation of carrier accumulation and relaxation regions, which allows remarkable enhancement of the gain. The structure consists of doped layers separated by 200 – 500 nm of pure-Ge. Vertical electric field (~ 1 - 2 kV/cm) and perpendicular magnetic field (~ 1 T) provide inversion population on direct intersubband light- to heavy-hole transitions. Heavy holes are found to transit the undoped layers quickly and to congregate mainly around the doped layers. Light holes, due to tighter magnetic confinement, are preferably accumulated within the undoped layers, whose reduced ionized impurity scattering rates allow higher total carrier concentrations, and therefore higher gain, in comparison to bulk p-Ge lasers. Preliminary results of the calculations show a possibility of laser operation at liquid nitrogen temperatures. Device design and diagnostics of CVD grown structure are presented. Combination of total internal reflection and quasi-optical cavity design provides high laser cavity Q.

INTRODUCTION

Recent semiconductor-laser developments in the terahertz range of the electromagnetic spectrum include intervalence band p-Ge lasers [1], Si lasers based on optically pumped donors [2], and quantum cascade lasers (QCL) [3-5]. A fundamental challenge for any THz solid-state laser is intrinsic far-IR absorption by lattice vibrations, which increases rapidly with temperature [6]. Operation of solid-state far-infrared lasers at elevated temperatures can be achieved only if the gain is sufficiently high. This requires high carrier density, but ionized impurity scattering and electron-electron interaction increase with density and generally work against the conditions needed for high gain. Improvements in QCL technology in overcoming these problems have been very rapid recently, with continuous wave output and operation temperatures above liquid nitrogen reported. However, because of high growth accuracy requirements, QCLs can be grown by technologically advanced molecular beam epitaxy method (MBE) only, which limits maximal structure thickness. To obtain high laser cavity Q at the long THz wavelengths, structures should ideally be thicker than the wavelength, which for 100 cm^{-1} and refraction index n ~ 4 has an order of magnitude of 25 μm.

The p-Ge lasers based on intersubband transitions in the valence band in bulk p-type doped Ge crystals operate at liquid helium temperatures in a wide spectral window (50 – 140 cm^{-1}) allowed by lattice absorption in Ge and free carrier absorption. The population inversion on direct optical transitions from light-to-heavy hole sub-bands grows for certain ratios of applied electric and magnetic fields when light holes are accumulated on closed trajectories below the optical phonon energy, while heavy holes undergo rapid optical phonon scattering.

A typical small signal gain in p-Ge lasers has broad band nature and usually does not exceed 0.1 cm^{-1}, which is smaller than the Ge lattice absorption at 77 K (Fig. 1). This limits p-Ge laser operation to liquid helium temperatures and creates difficulties to reach CW operation.

Terahertz for Military and Security Applications II, edited by R. Jennifer Hwu, Dwight L. Woolard,
Proceedings of SPIE Vol. 5411 (SPIE, Bellingham, WA, 2004)
0277-786X/04/$15 · doi: 10.1117/12.542565

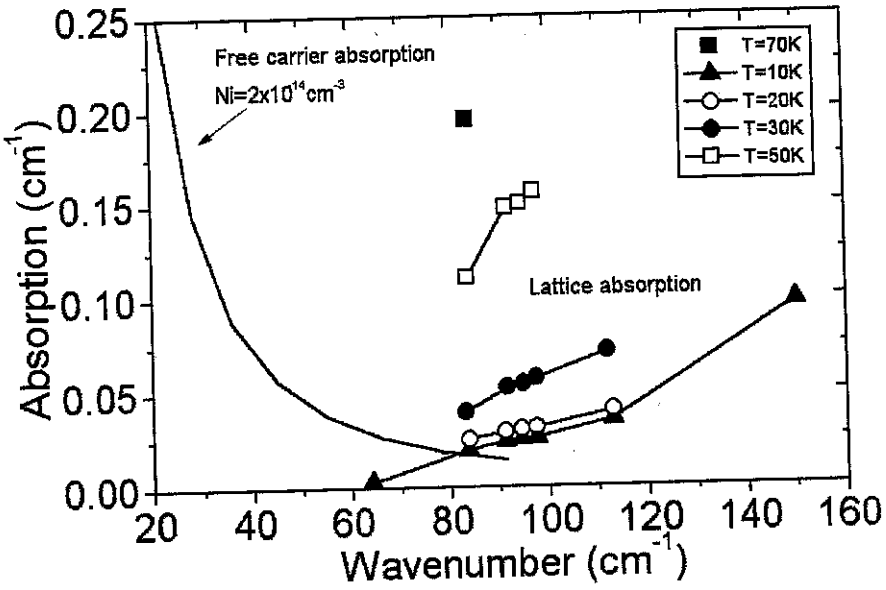

Fig. 1. Lattice absorption (from [6]) and typical free carrier absorption in Ge.

As an alternative to bulk p-Ge lasers, innovative structures composed of periodic doped and undoped regions of p-type semiconductor were studied in this work (Fig. 2). The spatial period of the structure was chosen smaller than the average Larmor radius of heavy hole trajectories in the crossed E and B fields, but larger than the average Larmor radius of light holes. Lower impurity scattering rates for light holes allow a remarkable increase of total carrier concentration in comparison to bulk p-Ge laser crystals and thus an increase in the gain. Higher gain is a key to achieving liquid nitrogen operation and CW operation.

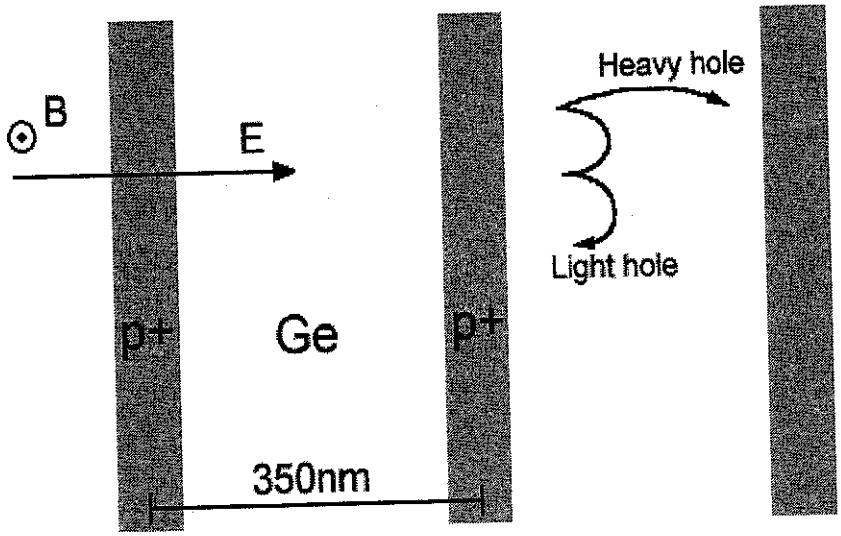

Fig. 2. Considered device structure. Carriers from p^+ layers are accelerated by the electric field (E) into cyclotron orbits determined by the perpendicular magnetic field (B). Fields are tuned so that the average light-hole orbits are smaller than the doping period while heavy holes suffer strong impurity scattering at the doped layers.

THEORETICAL METHODS

Monte Carlo simulation of carrier dynamics and far-infrared absorption was performed in considered structures (Fig. 2) using classical motion equations in external E and B fields and scattering probabilities to numerically solve the Boltzmann equation [7,8]. Time or ensemble averaged momentum and position yield the hole distribution functions $f_{l,h}(k,r)$ (sub-band (l,h), wavevector k and coordinate r). Two valence sub-bands (light and heavy holes) with isotropic and parabolic dispersion laws were considered. The period of the structure considered is ~ 350 nm and the typical magnetic field is ~ 1 T. Due to relatively thick structure period and moderate magnetic fields we can consider energy quantization due to magnetic field and confinement to be negligible, which permits a classical approach to the hole dispersion law and equations of motion. The standard Rees rejection technique chooses among scattering processes [7]. The rate of each scattering process is given by an analytic expression. Optical phonon scattering is treated in a deformation potential approximation [9,10]. Acoustic phonon scattering is simplified according to [11]. Inelasticity is included using [12].

The unscreened Ridley formula [13] with modified Brooks-Herring inter (intra) sub-band coefficients [12] is used for ionized impurity scattering. Considerations of quantum uncertainty for hole momentum were used for simulation of inter-sub-band tunneling during ionized impurity scattering. Statistically distributed solid angles of hole motion direction were used to calculate electron-electron scattering by a modification of the method that was used for ionized impurity scattering. These features in our MC procedure are new and differ from the approach to ionized impurity and electron-electron scattering that have been employed previously in p-Ge crystal laser simulations (see [14]). Besides being logically preferable, they predict results in better agreement with experiment than previous p-Ge laser MC simulations (see [15]) .

Monte Carlo code was specially written to include spatially varying scattering probabilities, which permitted simulation of carrier dynamics in media with stratified parameters, e.g. the structure with varying doping profile. For simulations presented here, the structure period d was chosen to be 350 nm. Introducing a "diffusion" profile of the doped layers simulates expected thermal diffusion of the dopant during CVD growth and also allows to neglect penetration of impurity scattering potential into undoped regions if characteristic diffusion length is larger than the square root of the typical impurity scattering cross section. Geometry of the structure allows the infinite charged planes approximation (size of the sample in the directions perpendicular to doped layers is very large compared to structure period).

Preliminary calculations indicated that redistribution of space charge influences the carrier dynamics at average concentrations above 10^{14} cm^{-3} at considered structure periods of 350 - 400 nm. The redistribution of space charge was included in the form of an additional "internal" electric field. Iteration was used to find self-consistent solution of the Poisson equation and thereof the spatial carrier distribution and potential profile. Total electric field across the structure is given by $E = -\partial\varphi/\partial x = E_{int} + E_{ext}$, where E_{ext} is the applied external field, and φ is electric potential. For any distribution of holes p(x) and negatively charged acceptor impurity centers N(x), the internal electric field along the period of the structure d is given by:

$$E_{int}(x) = E_0 + \frac{e}{\varepsilon\varepsilon_0}\int_0^x (p(x) - N(x))dx \qquad (1)$$

where ε is the relative dielectric constant, ε_0 is the permittivity of free space, and e is the electron charge. Due to periodicity and total neutrality of the crystal

$$E_{int}(x) = E_{int}(x + d) \qquad (2)$$

$$\int_0^d E_{int}(x) = 0 \qquad (3)$$

Small signal gain is calculated from the negative absorption of radiation due to direct inter subband (light to heavy) transitions and free carrier absorption assisted by phonons or ionized impurities [12]. In this case the absorption cross-section is proportional the integral over k of the difference $z_{lh}(k)[f_h(k,r) - f_l(k,r)]\delta(e_l(k) - e_h(k) - h\nu)$, where the distribution functions $f_{l,h}(k,r)$ for light and heavy holes are simulation outputs, $e_{l,h}(k)$ are hole energies, and $z_{lh}(k)$ is the unpolarized oscillator strength [16]. The total absorption cross section due to indirect transitions is given by the integral over the total indirect transition probability from an initial state (n,k,r) to all possible final states (n',k',r) due to absorption or emission of a photon, assisted by scattering.

CALCULATION RESULTS

Each period of the considered structure consisted of 0.8d pure germanium ($2.6*10^{13}$ cm^{-3}) acceptor concentration) and 0.2d doped at concentrations $3.5*10^{14}$ - $5*10^{15}$ cm^{-3}. This results in an average hole and acceptor concentration $N_{av} = 9*10^{13}$ - $1*10^{15}$ cm^{-3} (zero compensation is assumed). Doping profiles have been chosen in the form of the solution to the diffusion equation [17], simulating possible acceptor diffusion under high temperature conditions of CVD growth with possible values T = 750 C and 15 min duration (see Fig. 3).

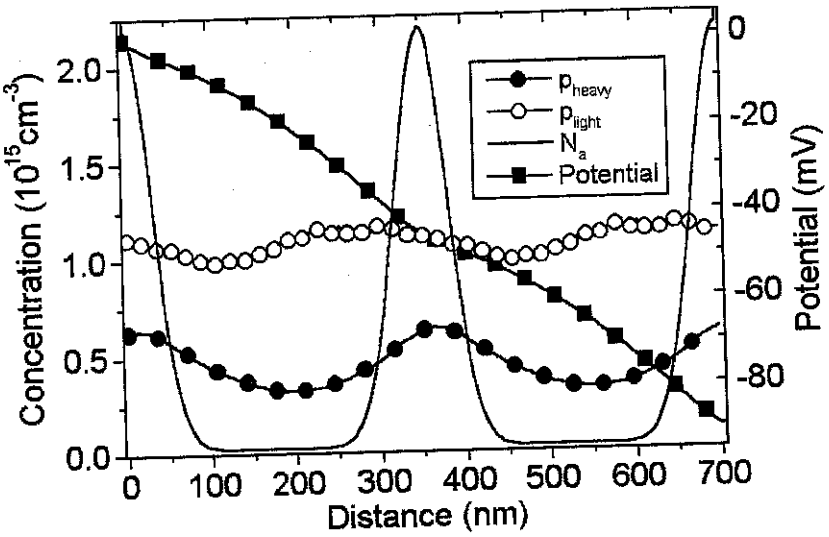

Fig. 3. Equilibrium potential distribution, concentration of light (multiplied by $(m_h/m_l)^{3/2}$)and heavy holes and acceptor concentration across the structure for applied fields E = 1.25 kV/cm, B = 1 T, T = 10 K and $N_{av} = 5*10^{14}$ cm^{-3}.

The spatial distribution of holes was investigated to determine the space charge and "internal" electric field distribution within the structure due to the static distribution of negative ionized impurity centers and the dynamic distribution of positive holes. For these particular simulations we assumed zero compensation, so that all introduced doping centers are shallow acceptors. Applied external fields are E = 1.25 kV/cm, B = 1 T, and the sample temperature is 10 K. By introducing appropriate initial p(x), this self-relaxation method converges to a stable distribution of holes p(x) with fixed acceptor distribution N(x). The internal field due to polarization of mobile holes and fixed acceptors is found to be comparable to the external one. The resulting total potential for $N_{av} = 5*10^{14}$ cm^{-3} is plotted in Fig. 3 as solid square symbols. The electric field is diminished in the first half of the structure period and augmented in the second (x > 170 nm). There is no potential well observed at this concentration. Light and heavy hole distributions are also plotted in Fig. 3. The light hole distribution is normalized using the relative density of states for light and heavy sub-bands (i. e. multiplied by $(m_h/m_l)^{3/2}$). The majority of holes are concentrated near the doped layers and most of them are heavy. At the same time, the distribution of light holes has a maximum near the central undoped region of the structure period, which creates strong inversion population there.

Fig. 4 compares the spatially averaged gain at 100 cm^{-1} for the considered structure for different average acceptor concentrations compared with similar results for bulk p-Ge crystal at T = 10 K (see [15]). As noted, the peak concentration value for the structure is more than 5x larger than found for bulk p-Ge crystal for the same conditions. The optical gain goes to zero quickly at concentrations above 10^{15} cm^{-3}. The optical gain maximum in the range 80 - 100 cm^{-1} for the structure is 4 times higher than the value for bulk p-Ge crystal.

Figs. 5 and 6 show results of gain calculations for the proposed structure at T = 77 K. The spectral-spatial far-IR gain distribution in strong applied electric and magnetic fields (E = 2.5 kV/cm, B = 2 T) is shown in Fig. 5. All negative gain points are truncated at zero level. Positive gain occurs in the spectral region 60 - 160 cm^{-1} with local maximum in the central region of the structure period between doped layers. Average gain over the structure is positive. Fig. 6 shows the spatially averaged gain spectrum for different applied electric and magnetic fields and for different average hole concentrations (zero compensation is assumed). Very strong phonon scattering at T = 77 K

increases optimal average hole concentration and applied-field magnitudes, required for to achieve positive gain. The value of the gain of 0.1 - 0.2 cm^{-1} at high applied fields has the same order of magnitude as published [6] lattice absorption at T = 77K (Fig. 1), which gives a promise for the possibility of laser operation in liquid nitrogen temperatures.

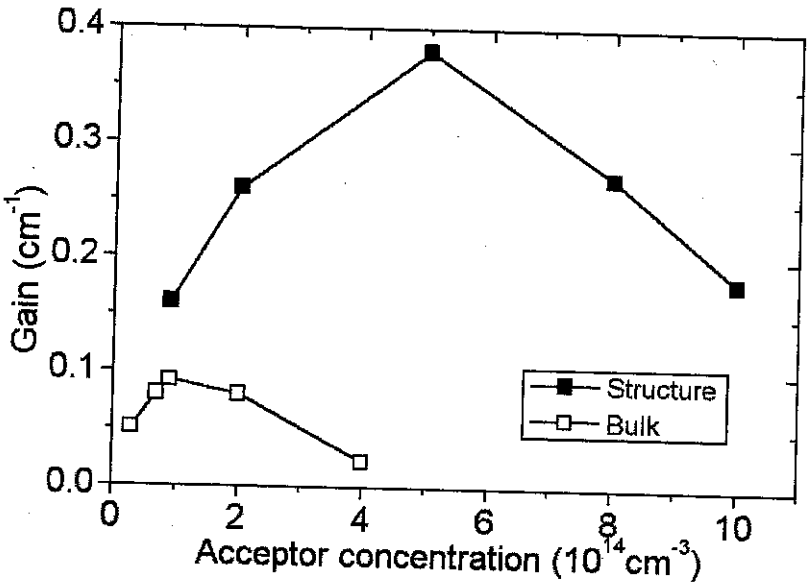

Fig. 4. Spatially averaged gain at 100 cm^{-1} vs. average hole concentration for selectively doped structure and bulk crystal for zero compensation at E = 1.25 kV/cm, B = 1 T, T = 10 K.

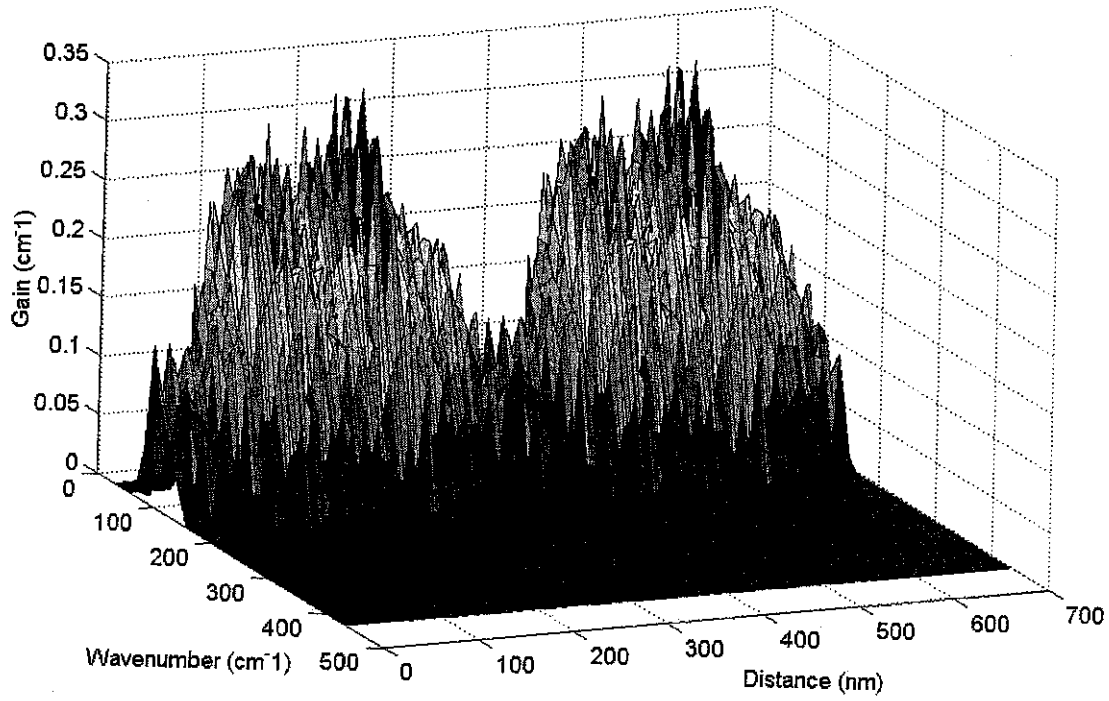

Fig. 5. Gain spectrum distribution across two periods of the structure for E = 2.5 kV/cm, B = 2 T, T = 77 K and average hole concentration $N_{av} = 8*10^{14} cm^{-3}$.

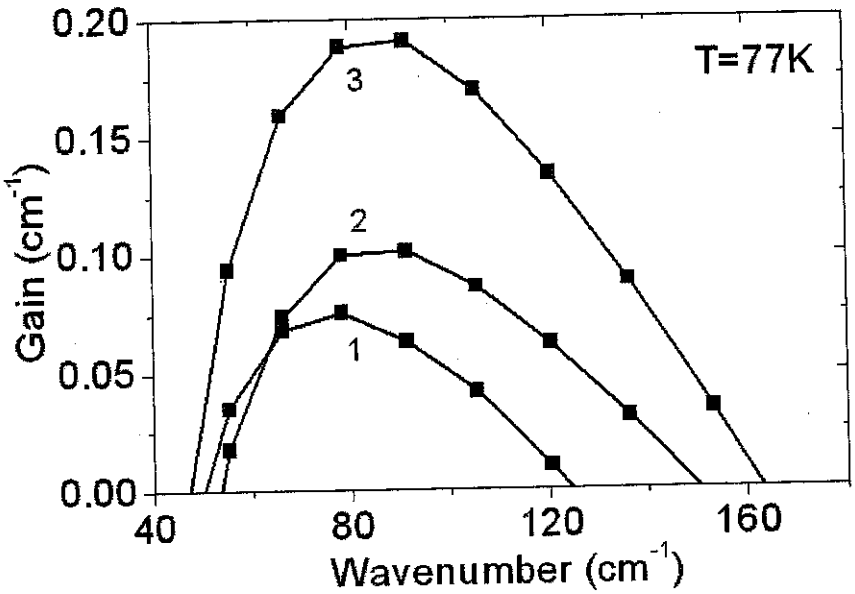

Fig. 6. Spatially averaged gain spectra for selectively doped structure at T = 77K. 1) E = 1.5 kV/cm, B = 1.2 T, $N_{av} = 5*10^{14}$ cm^{-3} 2) E = 2 kV/cm, B = 1.5 T, $N_{av} = 5*10^{14}$ cm^{-3} 3) E = 2.5 kV/cm, B = 2 T, $N_{av} = 8*10^{14}$ cm^{-3}.

DEVICE DESIGN

The considered structure will consist of periodic Ge:B doped layers ~ 40 nm thick separated by ~ 400 nm pure Ge regions. Boron concentration in the doped layers of $5*10^{15}$ cm^{-3} will provides $5*10^{14}$ cm^{-3} average carrier concentration. Electric field will be applied in vertical direction perpendicular to the layers and magnetic field will be applied along the layers. The simplicity and low growth precision requirements allow chemical vapor deposition (CVD), which can produce structures of remarkable active thickness compared to MBE-growth. We plan total active layer thickness of up to 100 μm, which is more than the estimated mode size for 1 mm length cavity. That will minimize electrodynamic cavity losses that have been one of the main technical challenges in THz QCLs. Also, in comparison with QCL, the considered Ge structure has a very broad gain spectrum of 50 - 140 cm^{-1}, so that stimulated emission can be tuned within the range by means of intracavity frequency selection.

Fig. 7 shows Secondary Ion Mass Spectrometer (SIMS) data taken from one of the test selectively doped structures. The structure consists of 35 periods with a total thickness of 14 μm. The linear SIMS spectrum in Fig. 7 shows more clearly the doping profile.

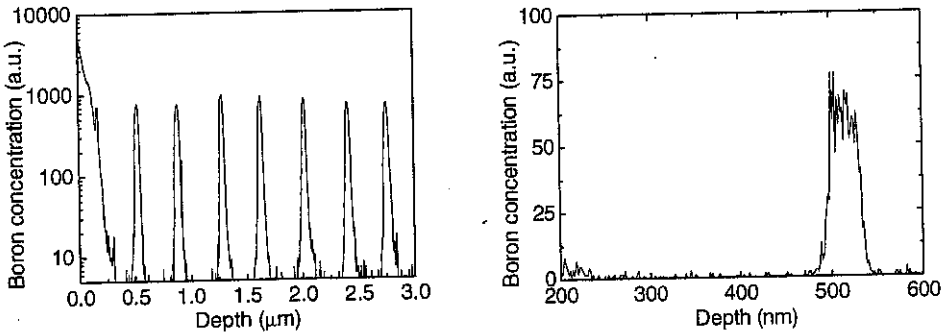

Fig. 7. **Left:** Semi-logarithmic SIMS spectrum of boron for first 7 periods of a CVD-grown 35 period p+Ge/Ge structure. The intentional high boron concentration on the surface is the contact layer. **Right:** Linear SIMS spectrum of the first period of the structure to determine the impurity diffusion profile.

Preliminary conductivity measurements at liquid helium temperatures revealed recharging effects inside the structure (Fig. 8), which indicate the negative differential conductivity region on I-V curves (see [18]). This effect is observed at relatively low electric fields only, and this should not lead to domain instability at the laser operation fields.

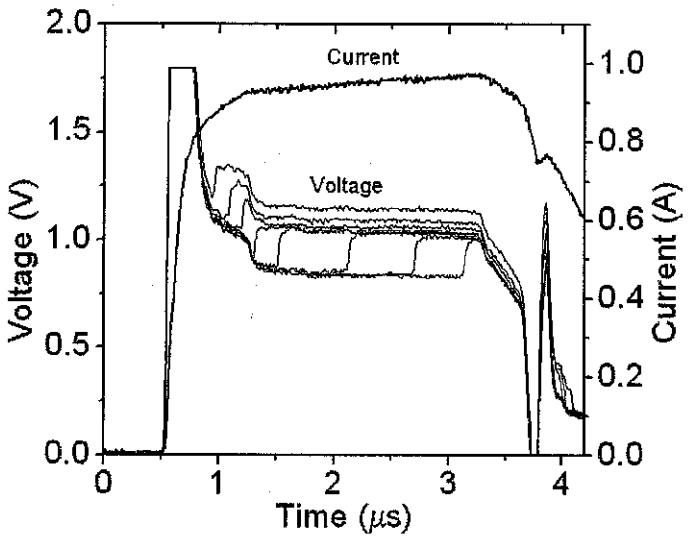

Fig. 8. Typical real-time traces of a voltage drop on the structure at 4 μs current pulse. Voltage traces correspond to different current values of 0.935 A, 0.943 A, 0.957 A, 0.964 A (shown), 0.967 A, 0.988 A, 1.016 A, 1.053 A (measured at t = 2.5 μs) from right to left. T = 4.2 K, B = 0.5 T

According to calculations, the pure Ge regions require an ionized impurity concentration below $3\text{-}5*10^{13}$ cm^{-3}. Our preliminary growth experiments, which produced a 10 μm thick Ge homoepitial layer, demonstrated that this purity level is achievable by CVD. This was verified by electron beam induced current (EBIC) measurements, which determine the minority carrier diffusion length, a function of impurity concentration. Diffusion length for the grown sample was compared to a calibration curve obtained using Ge standards, and the net impurity concentration was found to be about 10^{13} cm^{-3}. Fig. 9 presents a TEM image of a CVD germanium test sample to show the high quality of grown films.

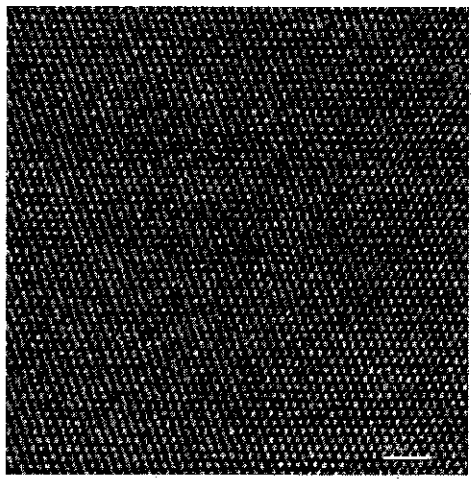

Fig. 9. HRTEM image of within 10 μm thick pure CVD-grown germanium on p-Ge substrate. This and similar pictures were taken spanning the expected epilayer/substrate interface ~ 10 μm below the wafer surface. No defects or dislocations were seen within the lattice of the crystal, indicating the high crystal quality of CVD Ge epilayers.

The multilayer Ge stack will be etched to form mm-size square mesas (Fig. 10). At the thicknesses of the structure close to 100 μm we can use quasi-optical approach to the electrodynamic cavity design. Lateral sides of the structure will be etched to have smooth cylindrical shape with ~ 1 mm curvature to provide mode confinement in vertical direction. In horizontal direction the mode is locked due to total internal reflections (Fig.10). Upper and lower contacts of the structure will be made using gold evaporation so that our actual cavity design will incorporate the QCL's double-sided-metal waveguide concept [3] in combination with a total internal reflection configuration. Our estimated electrodynamic loss in the proposed 1 mm^2 x 100 μm structure is 0.1 cm^{-1}, which is significantly less than the preliminary gain expectation of 0.4 cm^{-1}.

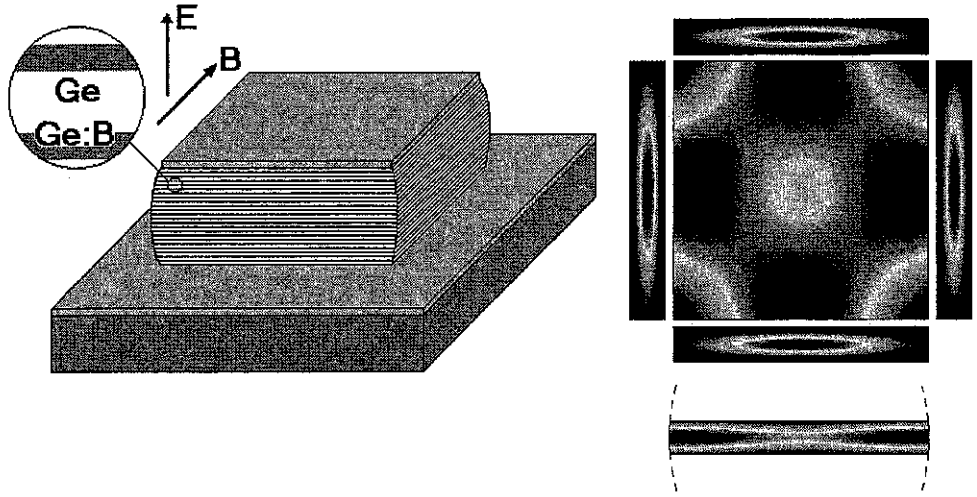

Fig. 10. **Left:** Rectangular mesa structure with double metal wave-guides and total internal reflection cavity design. Mesa walls are curved to provide better vertical mode confinement to minimize loses on metal layers. **Right:** Estimated mode distribution in 1 mm^2 square mesa structure, top and side views. Central cross-section of mode structure in 100 μm thick active layer with curved side walls.

SUMMARY

The performed calculations show that THz gain on inter-sub-band hole transitions in crossed electric and magnetic fields in the considered periodically doped Ge structure starts to decrease at remarkably higher average doping concentrations than that for bulk crystal p-Ge laser. Thus, such a structure can provide ~ 4 times higher spatially averaged gain than bulk crystal. Spatial separation of light hole accumulation regions from doped regions makes this possible.

The calculations have been performed at T = 10 K for a structure consisting of ~ 70 nm wide doped layers separated by ~ 280nm wide pure Ge gaps, so that the period of structure is 350 nm. Applied electric and magnetic fields are 1.25 kV/cm and 1 T, respectively. The maximum calculated local gain is ~ 0.6 cm^{-1}, and the average gain is ~ 0.4 cm^{-1}, while for comparison maximum calculated gain in bulk p-Ge crystal is ~ 0.1 cm^{-1}.

Higher gain in selectively doped Ge structures permits smaller active volume and provides a planar realization of p-Ge laser, which facilitates heat extraction. At the same time, higher gain allows lower electric field threshold, and hence lower Joule heating. This will lead to higher duty cycle and perhaps to CW operation.

The simplicity of proposed structure and potential use of the CVD growth method permit structures of remarkable thickness compared to existing QCL structures grown by MBE. Also note, that in comparison with QCL, the considered Ge structure has a very broad gain spectrum of 50 - 200 cm^{-1}, so that stimulated THz emission can be tuned within this region by means of intra-cavity frequency selection.

The value of the gain calculated for T = 77 K in high applied electric and magnetic fields is promising for a possibility of the proposed laser operation at liquid nitrogen temperatures.

ACKNOWLEDGMENTS

This work was partially supported by subconracts on AFOSR STTR Phase I contract F49620-02-C-0025 and AFOSR STTR Phase II contract F49620-02-C-0027 to Zaubertek and by NSF grant ECS-0070228 to UCF. We thank Dr. Remco Strijbos for initial advice on the Monte Carlo technique, Dr. O.A.Kuznetsov and Prof. V.I.Vorotyntsev for test CVD structures fabrication, Dr. L. Chernyak and O. Lopatiuk for EBIC diagnostics, M. Klimov for SIMS diagnostics and Dr. R. Vanfleet for HRTEM diagnostics.

REFERENCES

1. E. Brundermann, "Widely tunable far-infrared hot-hole semiconductor lasers" in *Long wavelength infrared semiconductor lasers*, edited by Hong K. Choi (Wiley, NJ, 2004), pp. 279-343
2. S. G. Pavlov, Kh. Zhukavin, E. E. Orlova, V. N. Shastin, A. V. Kirsanov, H.-W. Huebers, K. Auien, H. Riemann, "Stimulated emission from donor transitions in silicon," *Phys. Rev. Lett.* **84**, 5220 (2000)
3. B. S. Williams, H. Callebaut, S. Kumar, Q. Hu, J. L. Reno, "3.4 THz quantum cascade laser based on longitudinal-optical-phonon scattering for depopulation," *Appl. Phys. Lett.* **82**, 1015 (2003)
4. R. Kohler, A. Tredicucci, F. Beltram, H. E. Beere, E. H. Linfield, A. G. Davies, D. A. Ritchie, R. C. Iotti and F. Rossi, "Terahertz semiconductor-heterostructure laser", *Nature* **417**, 156 (2002)
5. M. Rochat, L Ajili, H. Willenberg, J. Faist, H. Beere, G. Davies, E. Linfield, and D. Ritchie, "Low-threshold terahertz quantum-cascade lasers", *Appl. Phys. Lett.* **81**, 1381 (2002)
6. R. Brazis, F Keilmann, "Lattice absorption of Ge in the far infrared", *Solid State Communications,* **70**, 1109, (1989)
7. C. Jacoboni and L. Reggiani, "The Monte Carlo method for the solution of charge transport in semiconductors with applications of covalent materials," *Rev. Mod. Phys.* **55**, 645 (1983)
8. C. Jacoboni, R. Brunetti and P. Bordone, "Monte Carlo simulation of semiconductor transport," in *Theory of Transport Properties of Semiconductor Nanostructures*, ed. Eckehard Scholl, (Chapman & Hall, London, 1998), p. 59
9. G. L. Bir and G. E. Pikus, *Symmetry and strain-induced effects in semiconductors*, (Wiley, NY, 1974).
10. P. Lawaetz, "Low-field mobility and galvanomagnetic properties of holes in germanium with phonon scattering", *Phys Rev.* **174**, 867 (1968)
11. J. D. Wiley, "Polar mobility of holes in II-V compounds," *Phys. Rev. B* **4**, 2485 (1970)
12. E.V.Starikov, P.N.Shiktorov, "Numerical simulation of far infrared emission under population inversion of hot sub-bands", *Optical and Quantum Electronics*, **23**, S177, (1991)
13. B. K. Ridley, "Reconciliation of the Conwell-Weisskopf and Brooks-Herring formulae for charged-impurity scattering in semiconductors: Third-body interference", *J. Phys. C: Solid State Phys.*,**10**, p. 1589, 1977
14. V. N. Shastin, "Hot hole inter-sub-band transition p-Ge FIR laser", *Opt. Quantum Electron.*, **23** pp. S111-S131, (1991)
15. M. V. Dolguikh, A. V. Muravjov, R. E. Peale, "Intervalence band THz laser in selectively-doped semiconductor structure" in "*Novel In-Plane Semiconductor Lasers III*" edited by C. F. Gmachl and D. P. Bour, Proc SPIE **5365**, 22 in press (2004)
16. Yu T. Rebane, "Sum rules for oscillator strength of intersubband and intrasubband transitions of free holes in cubic semiconductors", *Sov. Phys. Solid State* **25**, 1094 (1983)
17. W. C. Dunlap, Jr., "Diffusion of Impurities in Germanium", *Phys. Rev.* **94** 1531 (1954).
18. M. Rogozia, S. W. Teitsworth, H. T. Grahn, K. H. Ploog, "Relocation dynamics of domain boundaries in semiconductor superlattices", *Phys. Rev. B*, **65**, 205303 (2002)